Journal of Constructional Steel Research 177 (2021) 106475

Contents lists available at ScienceDirect

Journal of Constructional Steel Research

Low-frequency sinusoids for enhanced shear buckling performance of thin plates

Peter Y. Wang [a], Maria E.M. Garlock [a,*], Ted P. Zoli [b], Spencer E. Quiel [c]

[a] Princeton University, Dept. of Civil and Environmental Engineering, USA
[b] HNTB Corporation, New York Office, Empire State Building, 57th Floor, USA
[c] Lehigh University, Dept. of Civil and Environmental Engineering, USA

ARTICLE INFO

Article history:
Received 30 June 2020
Received in revised form 20 November 2020
Accepted 25 November 2020
Available online xxxx

Keywords:
Shear buckling
Corrugated web
Sinusoidal web
Plate girder
Thin steel plates

ABSTRACT

Thin plates subject to shear are ubiquitous in structures, used in webs of flexural members, shear walls, curved aircraft fuselages, ship hulls, etc. Given shear buckling concerns, these slender elements must be designed to balance plate depth and thickness. As slenderness limits capacity, strategies such as stiffeners or corrugations can enhance efficiency but are not without costs. In plate girder fabrication, the use of transverse and/or longitudinal stiffeners introduce poor fatigue details, while corrugation requires web forming and complex flange-to-web welding. The authors propose an alternative strategy, forming low-frequency sinusoidal (LFS) patterns along the plate's longitudinal axis as a novel, less fabrication-intensive approach to enhancing shear capacity of thin plates. The frequencies studied here are much lower than those used in commercial corrugated products and previous research, resulting in lower forming stresses, prospective fabrication using conventional semi-automatic welding techniques, and potentially improved fatigue behavior. Experimentally validated finite element models are used to evaluate sinusoidal frequency, amplitude, initial geometric imperfection, plate depth, and plate slenderness. Elastic shear buckling load, ultimate shear load, and shear yielding are used to evaluate effects of the parameters. Significant increases in shear strength and material efficiency can be achieved using an LFS approach. A standardized low-curvature LFS shape with 1.2 m wavelength is applicable to a wide range of plate depths and thicknesses without the need for specialized equipment to form the plate or weld the web-to-flange interface. LFS plates combine durability, material efficiency and ease of fabrication in a strategy that can benefit the industry.

1. Introduction

Structures that achieve strength using slender plates (such as deep beams, ships and aircraft) are often designed efficiently but may be limited by the shear buckling of their thin web plates; however, there is clear value to the use of slender webs, particularly if shear buckling can be eliminated as a failure mode. Slender plates (with slenderness defined as the plate depth to thickness ratio) can also give rise to reduced fatigue resistance and reduced resistance to corrosion that can compromise a structure's functional longevity [1–3]. Cyclic loading can cause thin plates in webs of deep beams (plate girders) to buckle in-and-out of plane (i.e. web breathing), potentially contributing to fatigue failure [2,4,5]. Slender plate girder design is often governed by web shear buckling, which initiates at the elastic shear buckling load, V_{cr} [6,7]. To resist web shear buckling, transverse (vertical) stiffeners are often welded onto the web plates at regular intervals to restrain lateral displacement at the panel boundaries and limit the width of potential buckling [8,9]. The space between vertical stiffeners is equal to "a" and defines the "panel." Stiffeners increase a web plate's V_{cr} by restraining out-of-plane displacement and reducing web panel aspect ratios to a/D, where D equals the web depth [8]. However, welded stiffeners have a variety of practical concerns such as installation (i.e. labor) costs and fatigue sensitivity [1,2]. Previous research by others has demonstrated that fatigue cracks in the web can initiate from the welds at the transverse stiffeners [2]. Therefore, strategies to reduce the use of transverse stiffeners would be beneficial to both girder construction cost and longevity.

An alternative to using transverse stiffeners is the corrugated plate. Corrugation in the direction of the girder span (perpendicular to the

Abbreviations: A, sinusoidal amplitude (distance from wave centerline to peak); D, web depth; E, Young's modulus; FE, finite element; FEM, finite element modeling; F_y, Yield stress; I_{t2}, stiffener postbuckling moment of inertia requirement from AASHTO; LFS, Low-frequency sinusoids /sinusoidal; TFA, Tension Field Action; V_{cr}, elastic shear buckling load; V_p, plastic shear strength; V_u, ultimate shear load; a, longitudinal length of panel, representing space between vertical stiffeners or cross bracing; a/D, web panel aspect ratio; b_f, flange width; f_n, normalized wave frequency; t_f, flange thickness; t_w, web thickness; τ_y, shear yield stress; ν, Poisson's ratio.

* Corresponding author.
E-mail addresses: pywang@princeton.edu (P.Y. Wang), mgarlock@princeton.edu (M.E.M. Garlock), tzoli@hntb.com (T.P. Zoli), seq213@lehigh.edu (S.E. Quiel).

https://doi.org/10.1016/j.jcsr.2020.106475

girder depth) can be imposed onto the web plate in the shape of trapezoids, triangles (zig-zags), or sinusoids [10]. Corrugation has been studied for decades to increase out-of-plane stiffness, thus increasing the web's shear buckling load and eliminating transverse stiffeners [9] [11]. Corrugated web plates have recently been used in select countries, with design described in Annex D of Eurocode 3, Part 1–5 [12], though their application has yet to gain acceptance in US practice [13–15]. When used in bridges, corrugated web designs have typically used a trapezoidal pattern [13,16,17]. However, sinusoidally corrugated web plates have demonstrated longer fatigue life than both conventionally-stiffened plates and trapezoidal corrugated webs [18–20]. This is because the smooth, continuous curvature in sinusoidally corrugated plates produces lower forming stresses and fewer stress concentrations than the sharp bend radii in trapezoidal corrugated plates [18,20]. The improved fatigue life offered by sinusoidal web patterns therefore warrants further study on sinusoidal plates.

Previous experimental and finite element studies by others have examined the failure mode of trapezoidal, zig-zag, and sinusoidal corrugated web plates for local buckling of individual folds, global buckling across folds, and a combination of the two in interactive buckling [11,14,20–24]. Most experiments have been conducted on trapezoidal web plates [14,21]. For sinusoidal corrugated plates, some experimental investigations [22,25–27] and parametric studies [20,24] have been carried out; however, tests focused on commercial products provided by specialized manufacturers, with the same fixed sinusoidal wavelength and amplitude [25–28]. Very little information has been published about the initial geometrical imperfections of these tested sinusoidal plates.

While the literature indicates that corrugated plates clearly enhance shear behavior, corrugated plates suffer from increased fabrication difficulty both in forming the plate and making the flange-to-web plate welds. Today's sinusoidal corrugated plate girder fabrication is achieved via an automated process whereby the web plate is cold-formed and then robotically welded to the flanges, as described by [11,29]. This technique is specialized and equipment-intensive [11,25,26,28,29]; for this reason, sections of prefabricated sinusoidal web I-girders are currently made to order from specialized manufacturers [11]. The technique also has implicit limits on plate girder depth and web plate thickness; the maximum sinusoidal web depth is 1.5 m, while the maximum sinusoidal web thickness is 6 mm [11]. Given the potential for corrosion and section loss, larger web plate thicknesses are often needed for bridges and other weathering applications [15,21,28,30]. Larger web depths and thicknesses are also needed for higher load demands.

This paper proposes a more constructible and potentially fatigue-resistant alternative to increase the shear buckling strength of thin plates by introducing low-frequency sinusoids (LFS). "Low-frequency" denotes sinusoids with a full wavelength on the order of 0.7 m or longer. In comparison, commercial sinusoidal corrugated web plates typically have a full wavelength of 0.155 m [11] (see Fig. 1). The proposed frequencies are thus much lower than those used in commercial corrugated web products and in previous research studies [11,20]. Few parametric studies on sinusoidal corrugation frequency have been conducted [20,24], and low corrugation frequencies approaching a flat plate have yet to be explored.

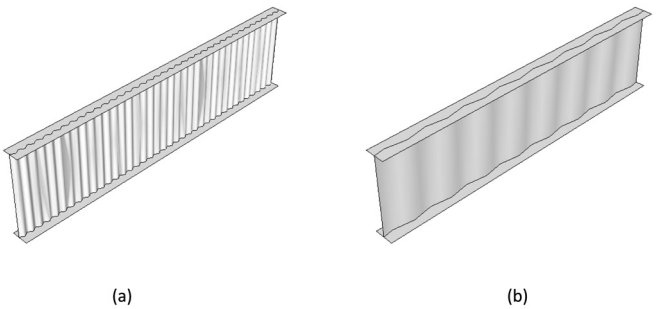

Fig. 1. Representative plate girders with a (a) typical corrugated web and (b) LFS web.

The web alteration to establish LFS geometry is defined by frequency and amplitude. A combination of low frequency and low amplitude can be largely beneficial to the fabrication process as well as structural performance and longevity. The difficulties associated with web forming are directly related to the forces necessary to deform the web and the number of forming steps; thus, reducing the sinusoid frequency can enable a simplified web-forming procedure, decrease forming stresses due to lower curvature, and broaden application to thicker webs [31]. In addition, the lower curvature of the LFS webs may still be accommodated by conventional flange-to-web welding approaches by adapting semi-automatic welding techniques, thus enabling conventional steel shops to fabricate LFS webs without specialized equipment.

The objective of the research presented herein is to evaluate the potential of low-frequency sinusoids (LFS) for enhancing the shear buckling performance of slender plates. The research also aims to extend the benefits of LFS to plate depths and thicknesses larger than that of corrugated plates. Experimentally validated finite element models (FEM) are used to perform a parametric study that evaluates the effects of sinusoidal wavelength (frequency), sinusoidal amplitude, initial geometric imperfection, girder depth, and web slenderness. Measurements of the elastic buckling shear load, ultimate shear load, and initiation of shear yielding are made to evaluate the effects of the various parameters.

2. Modeling approach and validation

A nonlinear finite element (FE) study was conducted using ABAQUS 2017 to analyze the behavior of several LFS web girder designs under pure shear [32]. The LFS geometries were modeled without considering any resulting forming stresses. Web panels with flanges were modeled with the boundary conditions and loading shown in Fig. 2, adapted from a previous study by Yoo and Lee to produce a state of pure shear [33]. The web is simply supported along its two vertical edges. The flanges are fully constrained to the top and bottom edges of the web at their interface to simulate the welds (tie constraints in ABAQUS). The web corners are rotationally fixed to represent continuity of the flange through the ends of the modeled panel length.

Uniformly distributed shear loads are applied along the four edges of the web plate as shown in Fig. 2. The load at the top and bottom of the web follows the shape of the sinusoid at its points of application.

The steel material model used for this study has a Young's modulus $E = 200$ GPa, yield stress $F_y = 345$ MPa, and Poisson's ratio $\nu = 0.3$. The steel is modeled as elastoplastic with strain-hardening defined by the Eurocode 3, Part 1–2 [34], as shown in Fig. 3.

ABAQUS shell elements of type S4 ("doubly-curved, general purpose, finite membrane strains") [32] are utilized with five integration points through the plate thickness (determined to be adequate for this application in the authors' previous work [35,36]). The FE mesh has a 4 cm maximum edge dimension (see Fig. 2), as determined by a previous convergence study on the elastic buckling load of a flat web panel [36].

A linear eigenvalue analysis is first performed to determine each girder's elastic shear buckling load (V_{cr}) and buckled eigenmode shapes. In the subsequent nonlinear analysis procedure, an initial geometric imperfection is applied to the web by overlaying a scaled value of the first shear buckling eigenmode geometry onto its finite element mesh. These imperfections (which are imposed with no additional stresses) numerically allow the buckling bifurcation of the web plate in pure shear and account for the influence of realistic geometric imperfections [37,46]. In this study, the maximum magnitude of this initial imperfection is examined over a wide range: D/10,000, D/1000, D/400, and D/100 [36]. The smallest value (D/10,000) represents a negligible initial imperfection that still allows buckling to occur numerically in the finite element

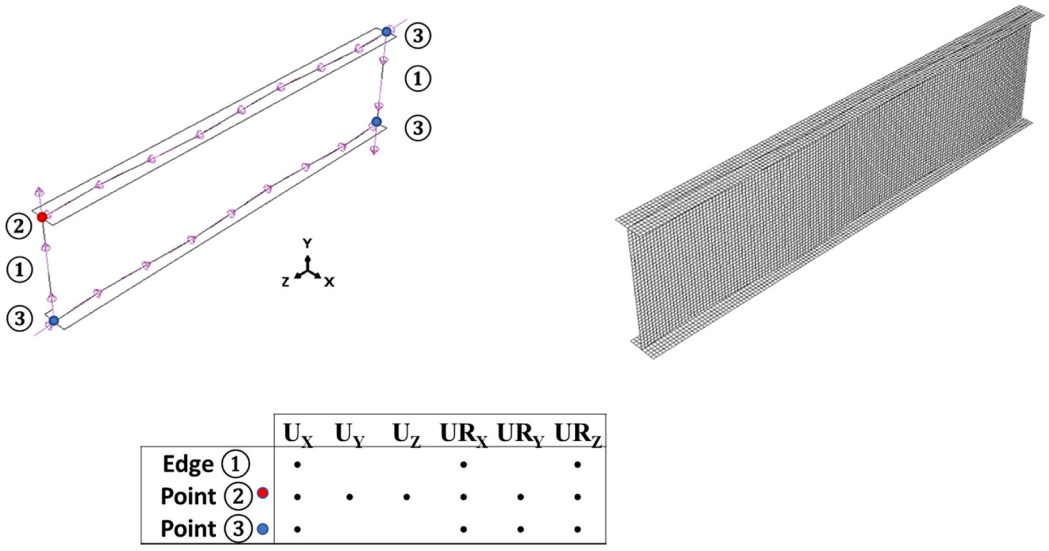

Fig. 2. Boundary conditions and pure shear loading on a representative LFS specimen with $f_n = 1$ (left), including finite element mesh with 4 cm mesh size (right). U denotes displacement, and UR denotes rotation.

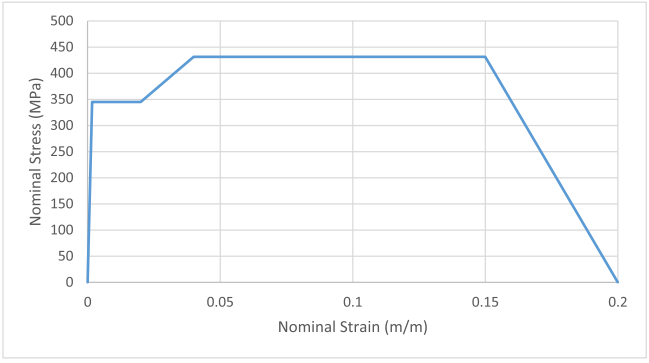

Fig. 3. Steel material model.

model, while $D/1000$ and D/400 represent more realistic imperfections per previous experimental measurements [14,21,26,38] and $D/100$ represents the largest initial imperfection within industry tolerance for flat webs per the D1.5 Bridge Welding Code of AASHTO and the American Welding Society [39]. Once initial imperfections are applied, each specimen is quasi-statically loaded (i.e. very slowly with negligible dynamic effect) to its ultimate shear load V_u using the Modified Riks nonlinear solver [32,37]. The ultimate shear load V_u was taken as the peak value in the shear load-displacement response [40].

This nonlinear FE modeling approach has been previously validated for several flat web girder specimens using the results of experimental tests by others [40]. Additional validations were conducted for this study using 8 experimental tests on sinusoidal corrugated web girder specimens from [22,25,28]. The FE model shown previously in Fig. 2 is adapted to the dimensions and geometry of each test specimen, which is summarized in Table 1. For the dimensions in Table 1, t_w is the web thickness, b_{f1} is the top flange width, t_{f1} is the top flange thickness, b_{f2} is the bottom flange width, and t_{f2} is the bottom flange thickness. All analyses utilize the aforementioned Eurocode 3 stress-strain relationship [34], using the F_y and E values from Table 1. Where available, the geometric imperfection magnitudes were modeled according to values reported from the tests [22,25,28]; if not reported, a generic imperfection magnitude of $D/400$ was assumed [21,38].

A comparison of ultimate shear strength V_u from FE analyses and experimental tests (V_u^{FE} and $V_{u,}^{exp}$ respectively) is provided in Table 2. Note that the V_u^{exp} values for reference [22] were extracted from its figures since no specific numerical values were reported. As demonstrated by the $V_u^{FE} / V_u{}^{exp}$ column, the FE predictions of V_u show good agreement with the corresponding experimental values. For 6 of the 8 specimens, the FE approach predicted V_u within 6% of the ultimate shear strength from experimental tests. For specimens S-1 and S-2, the FE models provide a V_u prediction that is 13–14% less than the experimental values. It is likely that this result was caused by material overstrength in the test specimens, as FE predictions by that study's authors [22] had an almost identical underprediction of V_u^{exp}.

Table 1
Material properties and dimensions of sinusoidal corrugated web girder specimens from experimental tests.

Specimen Name	F_y (MPa)	E (GPa)	wavelength (m)	amplitude A (cm) (see Fig. 4)	a (m)	D (m)	t_w (mm)	b_{f1} (mm)	t_{f1} (mm)	b_{f2} (mm)	t_{f2} (mm)
Pasternak et al. 2009 [28]	297	198.4	0.155	2	1.426	1.502	6	251 & 299[b]	12.6 & 12.4[b]	251 & 299[b]	12.6 & 12.5[b]
Pasternak et al. 1999 [25]	225	180	0.155	2	1.470	1.501	2.1	250	12.4	250.3	12.5
Guo et al. S-1 [22]	300	200[a]	0.155	2	0.75	0.500	2	200	10	=[c]	=[c]
Guo et al. S-2 [22]	300	200[a]	0.155	2	0.75	0.500	2.5	200	10	=[c]	=[c]
Guo et al. S-3 [22]	300	200[a]	0.155	2	0.75	0.750	2.5	250	12	=[c]	=[c]
Guo et al. S-4 [22]	300	200[a]	0.155	2.15	0.75	0.750	3	250	12	=[c]	=[c]
Guo et al. S-5 [22]	300	200[a]	0.155	2	1	1.000	2.5	300	12	=[c]	=[c]
Guo et al. S-6 [22]	300	200[a]	0.155	2.15	1	1.000	3	300	12	=[c]	=[c]

[a] the E value was not provided in [22], so a generic E value of 200 GPa was assumed.
[b] for the specimen from [28], the flange was composed of two stacked plates with widths and thicknesses shown.
[c] "=" means that the bottom flange dimensions (b_{f2}, t_{f2}) are equal to the top flange dimensions given (b_{f1}, t_{f1}).

Table 2
Comparison of finite element (FE) and experimental V_u values for sinusoidally corrugated web girder specimens.

Specimen name	V_u^{FE} (kN)	V_u^{exp} (kN)	V_u^{FE}/V_u^{exp}
Pasternak et al. 2009 [28]	1440	1358	1.06
Pasternak et al. 1999 [25]	377	365	1.03
Guo et al. S-1 [22]	163	190	0.86
Guo et al. S-2 [22]	207	238	0.87
Guo et al. S-3 [22]	316	326	0.97
Guo et al. S-4 [22]	382	390	0.98
Guo et al. S-5 [22]	416	428	0.97
Guo et al. S-6 [22]	503	494	1.02

3. Parametric study of LFS geometry

A parametric study was conducted to investigate the effect of sinusoidal frequency (wavelength) and amplitude on web shear buckling behavior of a prototype girder, which is based on the *FHWA Standard Plans for Highway Bridges* [41] with a web depth D = 1.473 m (58″) and web thickness t_w = 11 mm (7/16″) (resulting in web slenderness D/t_w = 133). The top and bottom flanges both have width b_f = 356 mm (14″) and thickness t_f = 27 mm (1–1/16″). The web panel aspect ratio (a/D) is given by the length of the web panel a over the web depth D. A panel length of 5.892 m (19 ft., 4 in), resulting in an a/D ratio of 4, was used to model the case of an unstiffened web. This panel length is close to the distance between cross-bracing from [41], which is 6.858 m (22′-6″). In general, an "unstiffened" plate in the context of this paper refers to a panel aspect ratio (a/D) greater than 3. Unstiffened flat plates have postbuckling shear capacity per Höglund [42] and recently adapted by Daley et al. [43] for the AISC specification [44]. Postbuckling shear capacity is characterized by the postbuckling reserve (defined as V_u- V_{cr}) [33].

The following parametric variations of the prototype girder are considered: normalized wave frequency (f_n) and sinusoidal amplitude (A) as shown in Fig. 4, the magnitude of initial geometric imperfections, web plate depth (D), and plate slenderness. Note that only the web plate is sinusoidal (and only in the longitudinal direction), while the flanges remain straight.

Fig. 4 illustrates the wave frequencies that are studied in the current paper. A normalized wave frequency (f_n) equal to 1.0 is defined as the wave pattern with one half sine wave over a distance of 1.473 m (i.e. the depth of the prototype web), as represented by Fig. 4(d). The minimum f_n chosen was 0 (corresponding to a flat plate) while the maximum f_n was 4.0 per Fig. 4(i) (which is less than a quarter of frequencies typically used for existing corrugated web designs [11]). Sinusoidal amplitude, A, measures the transverse distance from flange centerline to the peak of the sinusoid as shown in Fig. 4. Amplitudes range from 0 cm (flat plate) to 5 cm. Table 3 introduces the low-frequency sinusoidal (LFS) web geometries that are considered in this study and lists their full wavelengths. The nomenclature of the girder specimens is expressed as F#-A#, with the first value representing the normalized wave frequency f_n and the second value representing the amplitude in centimeters (see Fig. 4). In this study, the aforementioned dimensions of the prototype (D = 1.473 m, D/t_w = 133, length of the girder panel 5.892 m [19′-4″], b_f = 356 mm, t_f = 27 mm) are used unless otherwise noted.

3.1. Effects of wave frequency

The effects of wave frequency are examined by maintaining constant the initial geometric imperfection of D/400, amplitude A equal to 3 cm, and the prototype geometry (D = 1.473 m and web slenderness = 133). Table 4 lists the elastic shear buckling loads (V_{cr}) of girder specimens with different LFS web frequencies, and Fig. 5 presents an image of the first eigenmode for specimen F1-A3 and a flat web. It is seen

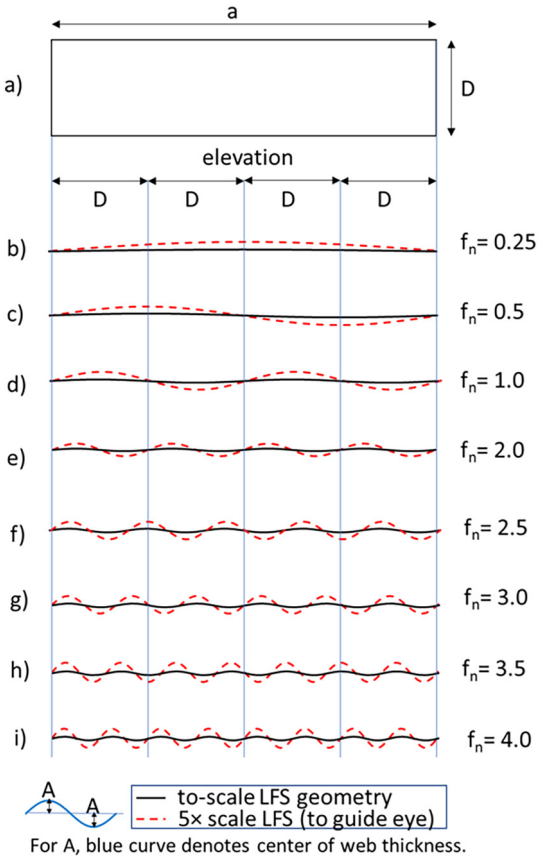

Fig. 4. Low-Frequency Sinusoidal (LFS) web geometry: a) elevation, b) to i) various normalized wave frequencies (f_n) and amplitudes (A).

that LFS web specimen F1-A3 has more antinodes than the flat web specimen, due to local fold buckling on the sinusoidal folds of the specimen. The shear buckling load V_{cr} of the flat web specimen is 1419 kN; by introducing two full sinusoidal waves into the web panel (f_n = 1), V_{cr} of specimen F1-A3 increases to 1937 kN, thereby achieving a substantial 37% increase in the elastic buckling load with low-curvature web forming. Table 4 indicates that this trend is consistent: the larger the f_n, the larger the V_{cr}.

Table 3
Parametric matrix of LFS frequency and amplitude in the prototype girder (with constant depth D = 1.473 m, web slenderness D/t_w = 133, and flange dimensions b_f = 356 mm, t_f = 27 mm).

Specimen Name	f_n (see Fig. 4)	wavelength (m)	amplitude A (cm) (see Fig. 4)
Flat web	0	N/A	0
F0.25-A3	0.25	11.784	3
F0.5-A3	0.5	5.892	3
F1-A3	1	2.946	3
F1.5-A3	1.5	1.964	3
F2-A3	2	1.473	3
F3-A3	3	0.982	3
F3.5-A3	3.5	0.842	3
F4-A3	4	0.737	3
F2.5-A1	2.5	1.178	1
F2.5-A2	2.5	1.178	2
F2.5-A2.5	2.5	1.178	2.5
F2.5-A3 (baseline)	2.5	1.178	3
F2.5-A4	2.5	1.178	4
F2.5-A5	2.5	1.178	5

Table 4
Summary of shear strength results for wave frequency variation (amplitude = 3 cm, depth = 1.473 m, web slenderness = 133, initial geometric imperfection of D/400).

Specimen name	f_n	V_{cr} (kN)	V_u (kN)	V_p (kN)	$\frac{V_u}{V_p}$
Flat web	0	1419	1694	3227	0.52
F0.25-A3	0.25	1425	1629	3227	0.50
F0.5-A3	0.5	1480	1555	3227	0.47
F1-A3	1	1937	1341	3227	0.42
F1.5-A3	1.5	2948	1968	3227	0.61
F2-A3	2	4399	2219	3227	0.69
F2.5-A3 (baseline)	2.5	6164	2759	3227	0.85
F3-A3	3	8462	2931	3227	0.91
F3.5-A3	3.5	10,440	3069	3227	0.95
F4-A3	4	11,873	3163	3227	0.98

Table 4 also summarizes the ultimate shear load V_u of the LFS web specimens and the plastic shear strength V_p of the web (an upper limit on the shear strength). The latter is calculated using the von Mises yield criterion, where τ_y is the shear yield stress:

$$V_p = \tau_y D t_w = \frac{1}{\sqrt{3}} F_y D t_w \quad (1)$$

The ratio V_u / V_p can be used as a measure of the efficiency of a corrugated web design; Sayed-Ahmed [13] suggests a value of 0.8 to 1.0 as the "optimum range" for "an efficient usage of steel." As shown in Table 4, the "Flat web" specimen achieves a V_u / V_p of only 0.52, specimen F2.5-A3 achieves 0.85, and F4-A3 approaches 1.0 with $V_u / V_p =$ 0.98. These results illustrate that LFS frequencies at or above $f_n = 2.5$ will efficiently utilize the web's steel material capacity.

3.2. Effects of initial imperfections

The effects of wave frequency discussed above were based on an initial geometric imperfection value of $D/400$. This section examines wave frequency with consideration of other initial imperfection magnitudes, since these imperfections will affect the shear strength in many cases. Fig. 6 evaluates the effects of both wave frequency and initial imperfection. Initial imperfection values of $D/10{,}000$, $D/1000$, $D/400$, and $D/100$ are considered as described in Section 2. The black dotted line (lowest) shows the AASHTO prediction for shear strength of the unstiffened flat web specimen (V_{cr} AASHTO), while the black solid line (top) shows the plastic shear strength (V_p) of the flat web specimen (see Eq. 1). In order to compare the strength of LFS webs to transversely stiffened webs, the black dashed line shows the AASHTO design capacity of a transversely stiffened $a/D = 2$ panel based on Tension Field Action (TFA) theory. This value of $a/D = 2$ implies that a vertical stiffener is

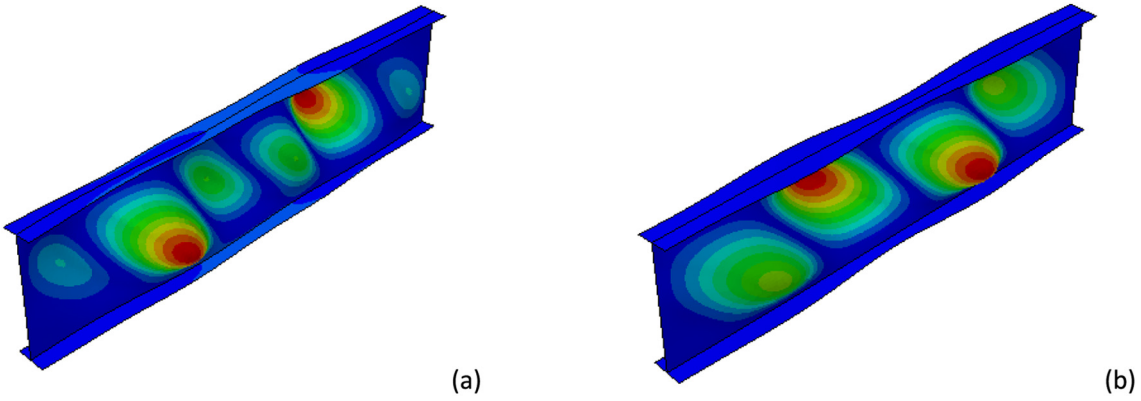

Fig. 5. First buckled eigenmode: comparison of flat web to LFS.

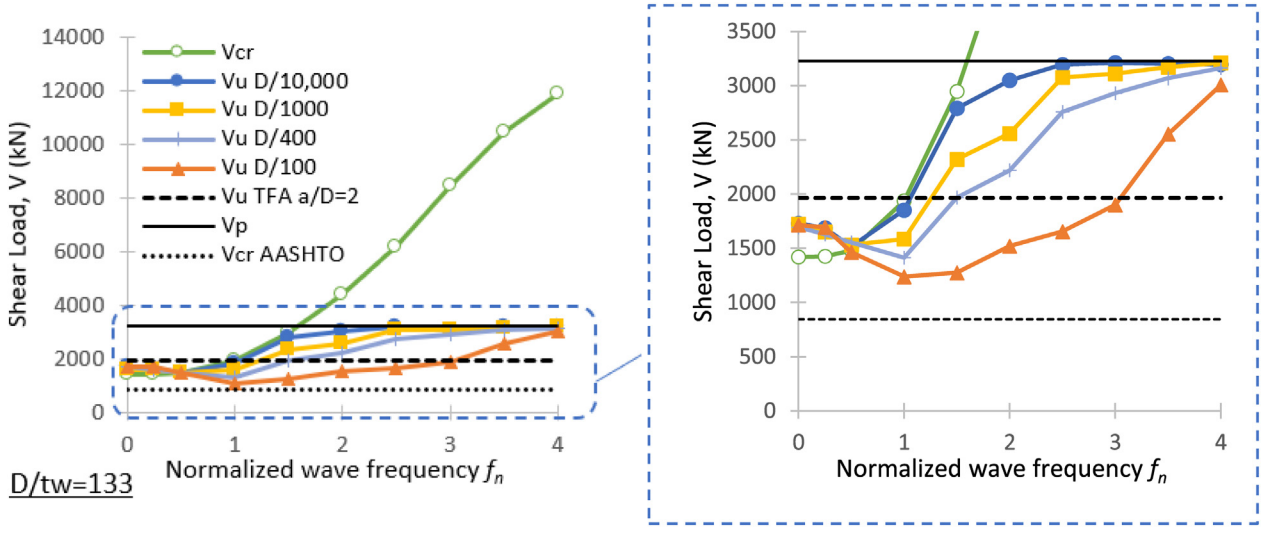

Fig. 6. Variations of normalized wave frequency and initial imperfection magnitude (amplitude = 3 cm, depth = 1.473 m, web slenderness = 133). Each f_n value corresponds to the specimen F[f_n]-A3. $f_n = 0$ corresponds to the "Flat web" specimen.

placed at the midlength of the flat web specimen (recall that the specimens studied here have $a/D = 4$ per Fig. 4).

In Fig. 6, V_{cr} represents the eigenvalue of the web plate, which is independent of imperfection value (since zero imperfection is used for the elastic eigenvalue analysis). Fig. 6 shows that V_{cr} grows dramatically (almost exponentially) with increasing wave frequency. Compared to the flat web girder (plotted as $f_n = 0$), minimal benefit in V_{cr} is observed for $f_n < 0.50$; however, V_{cr} exceeds V_p for f_n slightly larger than 1.5. In these cases, elastic buckling is ideally avoided and the inelastic limit state of V_u is reached [36,45].

Fig. 6 shows that both initial imperfections and wave frequency affect V_u significantly and thus will affect the postbuckling reserve (defined as V_u- V_{cr}). As stated previously, an imperfection magnitude of D/10,000 is much smaller than can be expected in practice, but it is sufficient to enable buckling in the numerical models. For this imperfection, the lower-frequency specimens (e.g. $f_n = 0$, 0.25, and 0.5) show V_u as higher than V_{cr}, and thus the plates have postbuckling reserve. For the intermediate frequencies tested (e.g. $f_n = 1.0$ and 1.5), V_u is virtually identical to V_{cr}, with negligible postbuckling reserve. In contrast, for $f_n = 2$ and above, V_u is lower than V_{cr} and V_u approaches the plastic shear strength V_p. The LFS web plate no longer buckles and is observed to reach full von Mises yield at its ultimate state. The $f_n = 2$ design has a significant (76%) increase in V_u compared to the flat web specimen ($f_n = 0$). The LFS web girders practically reach V_p (within 1%) for all specimens at $f_n = 2.5$ and above, implying that any higher frequency would practically achieve this plastic shear strength V_p result at this imperfection magnitude.

Fig. 6 also compares the ultimate shear load V_u vs. normalized wave frequency for other magnitudes of initial geometric imperfection. Recall that magnitudes of D/1000 and D/400 better represent what is expected in practice [21,38], and D/100 is an extreme case (at the threshold tolerance where any larger imperfection is not permitted by the American Welding Society) [39]. For typical imperfection magnitudes of D/1000 and D/400, LFS wave frequencies of $f_n = 2.5$ or above (i.e. with wavelengths below 1.2 m) allow V_u to approach the web's plastic shear strength V_p (achieving at least $0.85V_p$ as shown in Table 4). For the maximum imperfection tolerance of D/100, LFS wave frequency $f_n = 4$ (wavelength equal to 0.737 m) still allows V_u to reach a relatively efficient value of $0.93V_p$.

Overall, LFS designs with $f_n > 1.5$ match or exceed the shear strength of a flat web with a pair of transverse stiffeners at mid-panel ($a/D = 2$ as represented by the dotted dashed line). The only exception is the case for D/100, where the limit would be $f_n > 3$. These results suggest that examining the cost and durability tradeoffs of LFS webs versus welded stiffeners to achieve a desired shear capacity is warranted.

Fig. 7 plots the load vs. vertical displacement curves for some of the LFS specimens discussed in this section for an initial imperfection of D/10,000 and D/400. The D/10,000 plots, representing a negligible imperfection, isolate the effects of f_n on stiffness. Fig. 7 shows that the vertical shear stiffness of the girder remains unchanged by the sinusoidal wave frequencies up to LFS frequency $f_n = 2.5$. However, at higher LFS frequency $f_n = 4.0$, specimen F4-A3 shows a 22% decrease in shear stiffness. A difference in stiffness is observed for D/400 compared to D/10,000. Second-order bending effects due to increased out-of-plane imperfections tend to soften the shear stiffness of both flat and LFS specimens, yet the LFS web stiffnesses are still comparable to the flat web stiffness. Additionally, for D/400, LFS webs with higher f_n (e.g. 2.5 or 4) maintain their shear stiffness up to higher shear loads.

3.3. Effects of amplitude and initial imperfection

Next, the effect of wave amplitude, A, on the shear strength of the low-frequency sinusoidal (LFS) web girders is investigated using the last six specimens in Table 3 (maintaining constant the normalized wave frequency f_n equal to 2.5, and the prototype geometry with web depth $D = 1.473$ m and web slenderness = 133). Wave amplitudes

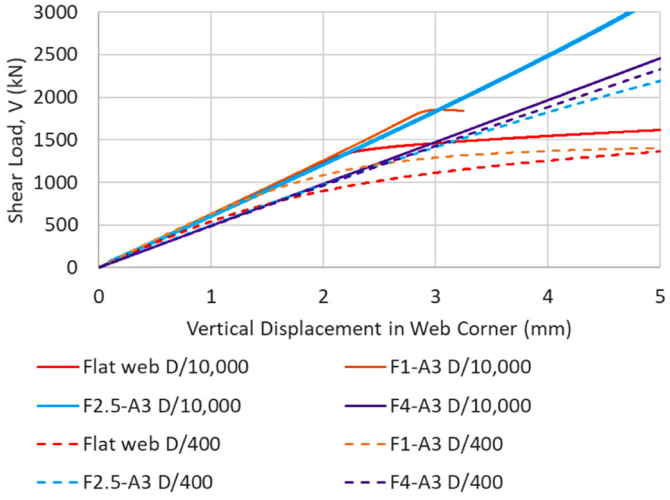

Fig. 7. *Load-displacement curves of select specimens with parametric frequency variations* (amplitude = 3 cm, depth = 1.473 m, web slenderness = 133).

from 0 cm to 5 cm were tested, where an amplitude of 0 cm represents the flat plate. Table 5 summarizes the numerical results for an assumed imperfection of D/400. It is observed that for all LFS specimens, V_u is significantly lower than V_{cr} – no postbuckling reserve therefore exists (V_u - V_{cr} = *negative*) for wave frequencies equal to 2.5 regardless of amplitude. It is also observed by the V_u/V_p ratio that V_u climbs closer to V_p as amplitude increases.

Fig. 8 plots the results of Table 5 and also includes the results of different imperfection magnitudes for the same specimens. Imperfection magnitudes of D/400 and D/100 equal 0.37 cm and 1.47 cm, respectively. It is seen that for these two imperfections, small amplitudes that are on the order of the imperfections can decrease V_u compared to the flat plate. For wave frequencies of 2.5, Fig. 8 shows that the amplitude should be at least three times larger than the expected imperfection for the LFS shear capacity to exceed that of the flat plate with a stiffener at midlength (i.e. V_u TFA $a/D = 2$ in the plot).

The increase of V_{cr} with amplitude is not as dramatic as it is with wave frequency (not exponential); therefore, frequency is clearly preferable. For example, starting from the "baseline" specimen that has a wave frequency $f_n = 2.5$ and amplitude 3 cm, raising the amplitude to 5 cm requires the same amount of material as taking the baseline and raising wave frequency to $f_n = 4$; however, the 5 cm amplitude geometry results in a V_{cr} of 7873 kN, while the $f_n = 4$ geometry gives a V_{cr} of 11,873 kN. Similarly, if an initial imperfection magnitude of D/100 is present, the 5 cm amplitude geometry only achieves a shear strength of $0.72V_p$, while $f_n = 4$ achieves a higher shear strength of $0.93V_p$. Therefore, incrementally higher wave frequencies are a more effective strategy for resisting elastic buckling and initial imperfections than larger wave amplitudes. In addition, larger amplitudes will lead to larger

Table 5
Summary of shear strength results for amplitude variation ($f_n = 2.5$, depth = 1.473 m, web slenderness = 133, initial geometrical imperfection of D/400).

Specimen name	Amplitude, A (cm)	V_{cr} (kN)	V_u (kN)	V_p (kN)	$\frac{V_u}{V_p}$
Flat web	0	1419	1694	3227	0.52
F2.5-A1	1	2748	1561	3227	0.48
F2.5-A2	2	4889	2519	3227	0.78
F2.5-A2.5	2.5	5594	2682	3227	0.83
F2.5-A3 (baseline)	3	6164	2759	3227	0.85
F2.5-A4	4	7120	2913	3227	0.90
F2.5-A5	5	7873	2929	3227	0.91

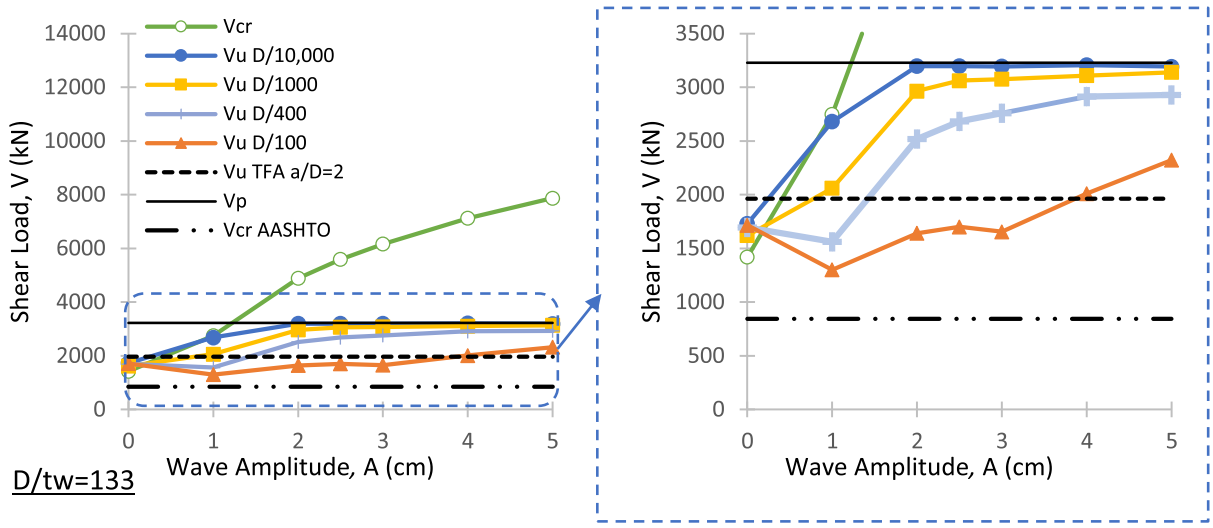

Fig. 8. Effects of wave amplitude on V_{cr} and V_u ($f_n = 2.5$, depth = 1.473 m, web slenderness = 133). Each amplitude A value corresponds to the specimen F2.5-[A]. A = 0 corresponds to the "Flat web" specimen.

transverse bending moment in the flanges, which is not as desirable for flange moment capacity [12].

Fig. 9 plots the load vs. vertical displacement curves for some of the LFS specimens discussed in this section for an initial imperfection of *D*/10,000 and *D*/400. The *D*/10,000 plots represent a negligible imperfection, permitting a clear evaluation of the effects of f_n on stiffness. It is seen that for *D*/10,000, the transverse shear stiffness remains the same for the LFS specimen with an amplitude up to 3 cm; however, at 5 cm amplitude, the shear stiffness decreases (decreasing by 23% compared to the flat web). Similar to findings from Fig. 7, a softening in shear stiffness is observed for *D*/400 compared to D/10,000 for both flat and LFS webs.

Shear deformations are currently deemed negligible by AASHTO's design criteria for flat web girders [30], so a small increase in shear deformation may not be significant. However, to conform with current code provisions, the largest LFS amplitude with near identical shear stiffness to a flat web girder would be preferable for design; an amplitude of 3 cm was thus maintained for the studies that follow in Section 4. Fig. 7 previously showed that LFS plates with frequencies below $f_n = 2.5$ (above wavelength 1.178 m) also exhibited a negligible

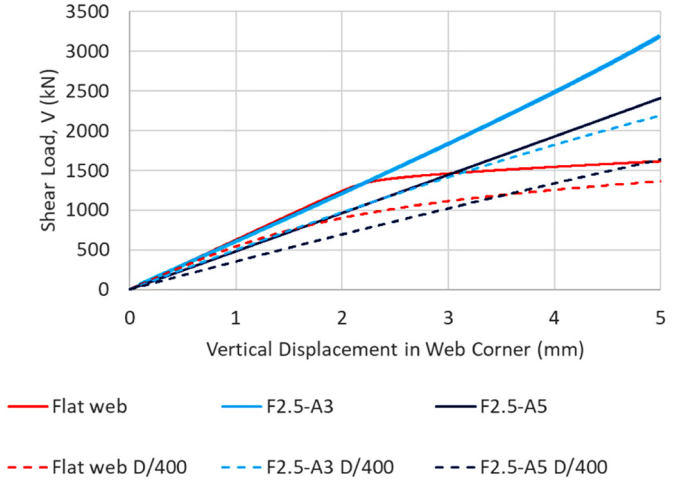

Fig. 9. Load-displacement curves of select specimens from parametric amplitude study on LFS web girders ($f_n = 2.5$, depth = 1.473 m, web slenderness = 133). Note the solid curves represent D/10,000 imperfection, while dashed curves represent D/400 imperfection.

effect on shear stiffness. Therefore, LFS web wavelength equal to 1.178 m and amplitude equal to 3 cm was selected as the desirable wavelength and amplitude for this depth and chosen as the *baseline LFS geometry* for Section 4's parametric study on web dimensions.

3.4. Material usage comparison

Table 6 compares the amount of steel required to fabricate each LFS web frequency to that required for an unstiffened flat web panel. The length of web (unfolded length of the sinusoid) is shown for each LFS web frequency for the prototype girder panel, which has a longitudinal panel length (*a*) equal to 5.892 m [19′-4″] (i.e. four times the depth). The weight of steel per longitudinal length is also determined for each LFS web frequency. The baseline LFS geometry (F2.5-A3) is only 0.6% heavier than the flat web specimen, but it has a significant 63% shear strength increase over the flat web assuming *D*/400 imperfection. It is seen that the highest LFS frequency ($f_n = 4$) is only ~2% longer than a flat plate, corresponding to a weight increase of less than 2.1 kg/m (less than 1.5 lb./ft) over the typical flat web. However, the corresponding strength increase is a significant 87% increase over the flat web. It is noted, however, that in a true beam, an aspect ratio of *a*/D = 4 will be subject to both shear and moment, where the LFS specimens will have a reduced plastic moment capacity compared to the flat plate specimen. Further discussion is given in Section 5.2.

4. Parametric study of web depths and slenderness

The "*baseline LFS geometry*" (amplitude = 3 cm and wavelength = 1.178 m) is used to study different web plate depths and thicknesses as summarized in Table 7. Recall that commercial sinusoidal corrugated webs are currently only fabricated to a maximum depth of 1.5 m and a maximum thickness of 6 mm [11,28]. The depths and thicknesses studied herein exceed these implicit limits to see if the LFS web can satisfy a new range of applicability. Another goal of studying various plate depths and thicknesses using the *baseline LFS geometry* is to determine whether this LFS configuration results in similar shear performance benefits across the different girder dimensions and can be used as a "*standardized LFS geometry*" (i.e. a geometry with the same wavelength and amplitude used for any selected depth and slenderness). Such findings would enable standardized fabrication of LFS geometries in girders with a range of web dimensions that more resembles girders deployed in current practice.

Table 6
Material quantity comparison for different wave frequencies f_n.

Specimen name	f_n	Length of web [a] (m) [ft]	Weight of steel[b] (kg/m) [lb/ft]	Length Ratio = Weight Ratio [c]	*Strength* V_u [d] (kN)	*Strength Ratio* [c]	V_u/V_p
Flat web	0	5.892 [19′–4″]	127.2 [85.5]	1.000	1694	1.00	0.52
F1-A3	1	5.898 [19′–4″]	127.3 [85.6]	1.001	1341	0.79	0.42
F2-A3	2	5.916 [19′–5″]	127.7 [85.8]	1.004	2219	1.31	0.69
F2.5-A3 (baseline)	2.5	5.930 [19′–5″]	128.0 [86.0]	1.006	2759	1.63	0.85
F3-A3	3	5.946 [19′–6″]	128.4 [86.3]	1.009	2931	1.73	0.91
F3.5-A3	3.5	5.965 [19′–7″]	128.8 [86.5]	1.012	3069	1.81	0.95
F4-A3	4	5.987 [19′–8″]	129.3 [86.9]	1.016	3163	1.87	0.98

[a] For 5.892 m segment between cross bracing.
[b] Average weight per unit length, based on 5.892 m segment between cross bracing.
[c] Normalized by flat panel, unstiffened ("Flat web").
[d] Determined from FEM with $D/400$ imperfection magnitude assumed.

As shown in Table 7, the baseline LFS geometry (herein given prefix "B" in nomenclature) is modified to examine various web depths ranging from 1.27 m to 2.946 m and web slenderness ranging from $D/t_w = 133$ (1.270 m web) to $D/t_w = 309$ (2.946 m web). Note that some specimens exceed the $D/t_w < 150$ slenderness limit recommended by AASHTO [30] to evaluate if LFS plates continue to maintain structural integrity with larger slenderness. Slenderness above 133 was achieved by raising web depth while keeping the web thickness constant at 9.5 mm (3/8″); this thickness was chosen to be above the minimum thickness allowed by AASHTO for corrosion concerns (5/16″ or ~ 8 mm) [30]. Depths of 1.27 m [50″], 1.473 m [58″], 1.905 m [75″], and 2.946 m [116″] are considered. The flange sizes for each depth were based on the FHWA reference discussed earlier in Section 3 [41]. Effects of depth are examined by maintaining constant an initial geometrical imperfection of $D/1000$ to reduce the influence of initial imperfections on these parametric results.

Table 7 tabulates the elastic buckling load V_{cr} and the ultimate shear load V_u achieved for each girder configuration. By using the baseline LFS geometry, the elastic buckling load V_{cr} of the specimens is always larger than the web's plastic shear strength V_p (See Eq. 1), regardless of girder depth and slenderness. In addition, with a small geometric imperfection of magnitude of $D/1000$, girders of all depths reach an ultimate shear load V_u greater than 89% of the web's plastic shear strength, except for slenderness equal to 309. At that high slenderness, the LFS web girder was still able to achieve 0.74 V_p, close to the recommendation of 0.8 V_p for the efficient design of corrugated webs [13]. At a constant slenderness of 133, the ratio of V_u / V_p remains between 0.94 and 0.98; it does not seem to be affected significantly by the depth. The slenderness appears to affect V_u / V_p more than the depth. These results suggest that the baseline LFS geometry (1.178 m full wavelength and 3 cm amplitude) has potential as a standardized LFS geometry for the range of plate depths and slenderness studied here.

5. Comparison with existing web-shear enhancement strategies

In this section, the performance of the LFS web configurations is compared against the two existing web shear strengthening approaches: corrugated plates and transverse stiffeners.

5.1. LFS vs. corrugated webs

LFS plates have longer wavelengths (>0.7 m) than commercial sinusoidal corrugated webs (0.155 m). However, they are also designed to be applied to a different range of plate thicknesses; LFS webs focus on thicker web plates associated with deeper girders and weathering applications (greater than 8 mm), while commercial sinusoidal corrugated webs focus on lower thickness web plates, from 2 mm to 6 mm [11]. Commercial products are fabricated to a maximum web thickness of 6 mm, although larger thicknesses would be necessary for bridges, cranes and other weathering applications to satisfy corrosion limits on thickness [30]. Table 8 shows a comparison of LFS patterns to the commercial sinusoidal corrugated web pattern for the different plate thicknesses shown. Both strategies are compared to the flat web plate of the prototype girder adapted from [41]. The shear strength V_u of each specimen was determined assuming a typical imperfection magnitude of $D/400$.

First, a comparison of the LFS patterns and the commercial pattern is conducted for a girder with an 11 mm thick web. Specimen F19-A2 represents a hypothetical sinusoidal corrugated web specimen ($f_n = 19.0$ [wavelength = 15.5 cm], amplitude $A = 2$ cm), with the same sinusoidal pattern as the commercial product but applied to a thicker plate (11 mm) than available commercially. If such a plate could be fabricated, it would achieve less than 0.5% strength increase over the highest performing LFS pattern (Specimen F4-A3) while being considerably more challenging to fabricate and 13% heavier. In addition, these webs would also garner significantly higher forming stresses that could reduce fatigue performance; it would be uneconomical to apply this commercial sinusoidal pattern to the thicker plate. The LFS configurations are thus better suited for this higher plate thickness.

The last row in the table represents the available commercial sinusoidally corrugated web product (Specimen "Commercial product"), which has a plate thickness of 6 mm. Six mm is the maximum thickness available commercially for these corrugated webs thus leading to a slenderness of 245 (compared to 133 for the 11 mm specimens). The commercial sine pattern allows the 6 mm web to achieve close to 95% of its plastic strength, showing it is well-suited for the smaller thickness. However, using a 6 mm plate for the LFS designs results in smaller

Table 7
Summary of web depth and slenderness study for baseline LFS (wavelength = 1.178 m and A = 3 cm) and D/1000 imperfection.

	Web dimensions			Flange dimensions		Shear Strength Results			
Specimen name	Depth D (m) [in]	Web thickness t_w (mm) [in]	Web slenderness D/t_w	b_f (mm) [in]	t_f (mm) [in]	V_{cr} (kN)	V_p (kN)	V_u (kN)	V_u / V_p
B-1.3D-133	1.270 [50]	9.5 [0.375]	133	356 [14]	27 [1.0625]	3978	2410	2274	0.94
B-1.5D-133 (prototype)	1.473 [58]	11.1 [0.4375]	133	356 [14]	27 [1.0625]	5782	3261	3195	0.98
B-1.9D-133	1.905 [75]	14.3 [0.5625]	133	356 [14]	27 [1.0625]	7914	5421	5188	0.96
B-3D-133	2.946 [116]	22.2 [0.875]	133	457 [18]	32 [1.25]	15,050	13,043	12,493	0.96
B-1.5D-155	1.473 [58]	9.5 [0.375]	155	356 [14]	27 [1.0625]	4927	2795	2546	0.91
B-1.9D-200	1.905 [75]	9.5 [0.375]	200	356 [14]	27 [1.0625]	4830	3614	3212	0.89
B-3D-309	2.946 [116]	9.5 [0.375]	309	457 [18]	32 [1.25]	6015	5590	4140	0.74

Table 8
Comparison of corrugated commercial web designs with LFS designs for 1.473 m deep girder.

Web Type	Specimen name	t_w (mm)	f_n	A (cm)	Length of web[a] (m) [ft]	Weight of steel[b] (kg/m) [lb/ft]	Length Ratio & Weight Ratio [c]	*Strength* V_u [d] (kN)	*Strength Ratio* [c]	V_u/V_p
Flat	Flat web	11	0	0	5.892 [19′-4″]	127.2 [85.5]	1.000 length 1.000 weight	1694	1.00	0.52
LFS	F2.5-A3 (baseline)	11	2.5	3	5.930 [19′-5″]	128.0 [86.0]	1.006 length 1.006 weight	2759	1.63	0.85
	F4-A3	11	4	3	5.987 [19′-8″]	129.3 [86.9]	1.016 length 1.016 weight	3163	1.87	0.98
	F2.5-A3-6mm	6	2.5	3	5.930 [19′-5″]	69.8 [46.9]	1.006 length 0.549 weight	896	0.53	0.51
	F4-A3-6mm	6	4	3	5.987 [19′-8″]	70.5 [47.4]	1.016 length 0.554 weight	1255	0.74	0.71
“corrugated”	F19-A2	11	19	2	6.765 [22′-2″]	146.0 [98.1]	1.148 length 1.148 weight	3178	1.88	0.98
	Commercial product	6	19	2	6.765 [22′-2″]	79.7 [53.5]	1.148 length 0.626 weight	1667	0.98	0.95

[a] For 5.892 m segment between cross bracing.
[b] Average weight per unit length, based on 5.892 m segment between cross bracing.
[c] Normalized by “Flat web” specimen.
[d] Determined from FEM with $D/400$ imperfection magnitude assumed.

strengths, lower than the flat plate with 11 mm. Thus, LFS designs are more viable for thicker plates when compared to corrugated plates.

It is interesting to compare the commercial product to the flat web and to the baseline LFS which has an 11 mm web thickness. It is seen that since the commercial product thickness is essentially half that of the other designs, it weighs less and also achieves essentially the same strength as the flat web (thus a tradeoff between cost of material and labor). In contrast, the baseline LFS is able to achieve 1.63 times the strength of the flat web with only a 0.6% increase in weight – essentially a negligible cost in material for a project. Both the baseline LFS and commercial product were successful in reaching a significant level of V_p for their plates (85% and 95%, respectively), whereas the flat plate only achieved 52% of V_p. For higher load demands and for higher thicknesses associated with weathering applications, the LFS strategy has thus shown potential.

5.2. LFS vs. welded transverse stiffeners

The most common approach for strengthening a web for shear capacity is to add transverse stiffeners. Table 9 compares the baseline LFS configuration to flat web prototypes with added stiffeners, where stiffener strategies are illustrated in Fig. 10. From a material standpoint, the different web stiffening strategies were compared to an unstiffened panel (over an assumed 5.892 m panel length between cross bracing).

Table 9 shows that a flat panel with a one-sided eccentric stiffener at mid length (designed for $a/D = 2$ per AASHTO [30]) uses 3% more material than an unstiffened flat panel, while a two-sided stiffener for $a/D = 2$ would be 4% more material than an unstiffened flat panel (though both stiffener cases will require additional labor for cutting and welding). To enforce an a/D ratio equal to 1 (square panels, see Fig. 10), 9% and 12% more material than a flat panel would be necessary for a designed one-sided stiffener and a two-sided stiffener, respectively. In contrast, the LFS web panel with the standardized configuration ($f_n = 2.5$) was only 0.6% more material than a flat panel. This is equivalent to only 0.8 kg/m [0.54 lb./ft] more weight than an unstiffened flat panel.

The ultimate shear strength of each web stiffening strategy was also compared in Table 9, as determined from FE modeling (assuming a typical imperfection magnitude of $D/400$). The LFS web strategy produces the greatest strength increase of 63% additional shear strength beyond that of an unstiffened flat panel. Thus, in addition to the benefits of reduced fatigue sensitivity and ease of fabrication from less cutting and welding, the LFS web strategy may be the strongest from a strength-to-weight perspective as well.

This study only considers the panel in pure shear. For an aspect ratio a/D = 4, both shear and moment would be expected in a realistic beam due to the increased length of the unstiffened web panel. While a study of shear-moment interaction is beyond the scope of this paper, it should be noted that LFS webs will reduce the plastic moment capacity of the beam since the web has a reduced axial stiffness. The aforementioned nonlinear finite element models in ABAQUS were used to determine the plastic moment capacities for the specimens with flat web and baseline LFS F2.5-A3 as 6735 kN-m and 5261 kN-m, respectively. In this case, the LFS beam therefore has 22% less plastic flexural capacity than the flat web beam. For comparison, the ABAQUS model of the corrugated web F19-A2 specimen indicated a plastic moment capacity of 4992 kN-m, and if one considers only the flanges (i.e., ignoring the web as is common for corrugated web design [12]), the calculated plastic capacity is further reduced to 4966 kN-m. This lower bound value represents a 26% drop in plastic capacity versus the flat web specimen. LFS and

Table 9
Comparison of material quantity and shear strength for different web-strengthening strategies for the prototype girder (tw = 11 mm, D = 1.473 m, slenderness = 133) (see Fig. 10).

Web type	a/D	Number of sides with stiffeners	Weight of steel[a] (kg/m) [lb/ft]	Weight Ratio[b]	Strength V_u[c] (kN)	Strength Ratio[b]
LFS (baseline, F2.5-A3)	4	unstiffened	128 [86.1]	1.006	2759	1.63
Flat web	4	unstiffened	127 [85.5]	1	1694	1.00
	2	1[d]	131 [88.1]	1.03	1789	1.06
		2[e]	132 [88.9]	1.04	1942	1.15
	1	1[d]	139 [93.5]	1.09	2242	1.32
		2[e]	142 [95.7]	1.12	2260	1.33

[a] Average weight per unit length, based on 5.892 m segment between cross-bracing.
[b] Normalized by flat panel, unstiffened.
[c] Determined from FEM with $D/400$ imperfection magnitude assumed.
[d] 1-sided stiffener (width 5″, thickness 9/16″) designed by AASHTO [30] to meet I_{t2} requirement.
[e] 2-sided stiffener (width 5″, thickness 3/8″) used in FHWA1982 Standard Plans [41] and designed by AASHTO [30] to meet I_{t2} requirement.

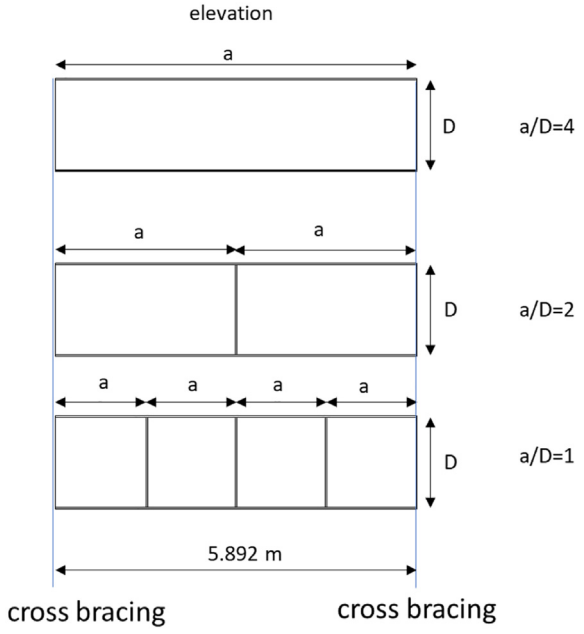

Fig. 10. Stiffener configurations for flat web prototypes presented in Table 9.

corrugated web designs are therefore most efficient under conditions of high shear and low moment (e.g. near supports of simply supported beams), with LFS webs providing only slightly more flexural capacity versus a corrugated web. If LFS beams are to be used in areas of high shear and high moment (e.g. over the supports of continuous beams), the flange strength should be enhanced by using larger plates and/or higher strength steel grades.

6. Summary and conclusions

This paper presented an efficient strategy for increasing the shear capacity of thin steel plates by introducing low-frequency sinusoids (LFS) along the plate's longitudinal axis, with wavelengths on the order of a meter. Experimentally validated nonlinear finite element models enabled a parametric study that examined the effects of two LFS parameters on the web of deep plate girders: the normalized wave frequency (f_n) and sinusoidal amplitude (A), where f_n is defined as the number of half sine waves in a distance 1.473 m (the depth of the prototype web), and A is measured from the flange centerline to the web's center of thickness at the sinusoidal peak. The effects of these LFS parameters were examined while varying the initial imperfection (out-of-flatness) of the LFS web plate and the web plate depth and slenderness (depth/thickness). Limit states such as elastic shear buckling load V_{cr}, ultimate shear load V_u, and the plastic shear strength V_p were recorded. In addition, V_u / V_p was evaluated as a measure of material usage efficiency, where a value of at least 0.8 is recommended for typical corrugated designs [13].

The following summarizes the results of the parametric computational study:

- Substantial increases in shear strength were achieved using LFS webs, improving ultimate shear capacity up to 87% over flat webs.
- Increasing f_n increases V_{cr} significantly. Generally, for f_n values greater than 1.5, an inelastic limit state such as V_u (sometimes nearly equaling V_p) is reached before V_{cr} is achieved.
- The assumed initial geometric imperfections (out-of-flatness) in the LFS web plate has a non-negligible effect on the shear strength of the plate. For example, for $f_n = 2.5$ and $A = 3$ cm, V_u for D/400 is 0.86 times that of V_u for D/10,000.
- For sinusoidal wave amplitudes of 3 cm, V_u / V_p ratios of 0.85 or larger are reached if frequencies $f_n = 2.5$ or greater are employed (given a typical $D/400$ imperfection), thus indicating that efficiencies equal to or greater than typical corrugated webs can be achieved using LFS.
- Frequencies and amplitudes had a negligible effect on the shear stiffness of the plate for f_n and A values less than or equal to 2.5 and 3 cm, respectively. Larger values decreased the shear stiffness.
- For the parameters studied, which only considers $a/D = 4$, the amplitude should be approximately three times larger than the expected imperfection magnitude for the LFS to have a benefit that exceeds the capacity of the flat plate with a stiffener at mid-length. Thus, considering the web depths and imperfections studied and assuming $f_n = 2.5$, amplitudes of 3 cm or larger are recommended.
- Increasing the wave frequency f_n has a much larger effect on shear capacity than increasing the amplitude for approximately equal material quantities.
- For f_n and A values equal to 2.5 and 3 cm, respectively, the evaluation of larger web depth and slenderness indicated that V_u / V_p ratios of 0.89 or larger are reached, with the exception being the most slender plate (slenderness = 309) which only achieved a ratio of 0.74.
- The amount of steel required to fabricate LFS web plates with A = 3 cm and f_n ranging from 1 to 4 is less than 1.02 times that of a flat plate.

In conclusion, the parametric computational study indicated that LFS plates lead to increased shear strength with negligible increase in material. Other notable advantages to this LFS strategy include relatively simple fabrication and eliminating welded stiffeners thus reducing fatigue sensitivity. These advantages imply an economical advantage as well. It is noted, however, that LFS webs will reduce the plastic moment capacity of the section on the order of 25%. LFS designs are thus most efficient in locations with high shear and low moment. Otherwise, the LFS flexural strength can be enhanced with larger flange plates and/or larger flange yield stress material.

This study also sought to ascertain a standard LFS design (wavelength and amplitude) that could be effective for various plate depths and slenderness. Such a standardized approach could eventually result in more cost-effective fabrication, as LFS web-forming and welding could be standardized. Analyses showed that an amplitude equal to 3 cm and a wavelength equal to about 1.178 m are optimal for girders with depths varying from 1.25 m to 3 m (and potentially deeper). This LFS configuration is selected based on shear stiffness, ultimate shear load V_u, the plastic shear strength V_p, and V_u / V_p (as a measure of efficiency). The analyses also show that the LFS pattern may be more suitable for higher depths and thicknesses than currently available commercial sinusoidal corrugated webs, expanding the range of applicability of sinusoidal webs.

The strength and efficiency of LFS plates were compared with standard plate strength enhancement approaches such as corrugated webs and transverse stiffeners. LFS plates have wave frequencies that are much lower than those used in commercial corrugated plate products – on the order of 8 times lower, and thus LFS requires much less material than corrugated webs assuming the same plate thickness. However, LFS plates match the shear capacity of corrugated plates only when applied to thicker plates, leading to the conclusion that LFS webs are more efficient for the larger plate thicknesses (on the order of 10 mm [greater than a quarter inch]), while commercial patterns are more suitable for lower thickness (6 mm or less). Compared to conventional corrugated webs, the LFS geometry reduces the amount of required forming, thus reducing forming stresses and stress concentrations and potentially benefitting fatigue performance. LFS has shown advantages over transverse stiffeners as well. Compared to adding stiffeners, for wavelength and A values equal to 1.178 m and 3 cm, the LFS design achieves 1.63 times the V_u of flat plates; however, if 3 stiffeners were added on each side of the plate at equal distance (enforcing $a/D = 1$), only an increase of 1.33 is observed (assuming typical $D/400$ imperfection).

Overall, this work concludes that LFS are a viable alternative to traditional shear strength enhancing strategies for thin plates such as corrugations and transverse stiffeners. A significant shear strength beyond that of a flat plate can be achieved through these low-frequency sinusoids and more research is warranted to develop design recommendations. Such future research includes experimental studies, examining combined moment and shear, boundary condition effects, fatigue life, and fabrication-induced initial imperfection shapes.

Declaration of Competing Interest

The authors declare that they have no known competing financial interests or personal relationships that could have appeared to influence the work reported in this paper.

Acknowledgements

This research was sponsored by the National Science Foundation (NSF) under grants CMMI-1662886 and CMMI-1662964. All opinions expressed in this paper are the authors' and do not necessarily reflect the policies and views of the sponsors.

References

[1] K. Balaji Rao, M. Anoop, G. Raghava, M. Prakash, A. Rajadurai, Probabilistic fatigue life analysis of welded steel plate railway bridge girders using S–N curve approach, Proceed. Institut. Mech. Eng. Part O J. Risk Reliability. 227 (4) (2013) 385–404.
[2] M. Skaloud, Breathing-induced fatigue in thin-walled construction, Procedia Eng. 66 (2013) 383–392.
[3] H. Günther, U. Kuhlmann, Numerical studies on web breathing of unstiffened and stiffened plate girders, J. Constr. Steel Res. 60 (3–5) (2004) 549–559.
[4] R. Crocetti, Web breathing of full-scale slender I-girders subjected to combined action of bending and shear, J. Constr. Steel Res. 59 (3) (2003) 271–290.
[5] M. Yaghoubshahi, M. Alinia, A. Milani, Master S-N curve approach to fatigue prediction of breathing web panels, J. Constr. Steel Res. 128 (2017) 789–799.
[6] S.P. Timoshenko, J.M. Gere, Theory of Elastic Stability, McGraw-Hill, Toronto, 1961.
[7] S.C. Lee, J.S. Davidson, C.H. Yoo, Shear buckling coefficients of plate girder web panels, Comput. Struct. 59 (5) (1996) 789–795.
[8] F. Bleich, Buckling Strength of Metal Structures, McGraw-Hill, New York, 1952.
[9] Y.D. Kim, D.W. White, Transverse stiffener requirements to develop shear-buckling and postbuckling resistance of steel I-girders, J. Struct. Eng. 140 (4) (2014).
[10] F. Riahi, A. Behravesh, M. Yousefzadeh Fard, A. Armaghani, Shear buckling analysis of steel flat and corrugated web I-girders, KSCE J. Civ. Eng. 22 (12) (2018) 5058–5073.
[11] H. Pasternak, G. Kubieniec, Plate girders with corrugated webs, J. Civ. Eng. Manag. 16 (2) (2010) 166–171.
[12] CEN, Part 1-5: Plated structural elements. Annex D (informative)- Plate girders with corrugated webs, *EN 1993-1-5 (2006) (English): Eurocode 3: Design of steel structures*, Brussels 2006, pp. 45–52.
[13] E.Y. Sayed-Ahmed, Corrugated Steel Web Plate / Box Girders: Bridges of the 21st Century, December 1998.
[14] J. Moon, J. Yi, B.H. Choi, H.-E. Lee, Shear strength and design of trapezoidally corrugated steel webs, J. Constr. Steel Res. 65 (2009) 1198–1205.
[15] H. Abbas, Analysis and Design of Corrugated Web I-Girders for Bridges using High Performance Steel, Proquest Information and Learning Company, 2003.
[16] R. Sause, H.H. Abbas, W.G. Wassef, R.G. Driver, M. Elgaaly, Corrugated Web Girder Shape and Strength Criteria, ATLSS Reports. ATLSS report number 03-18 2003.
[17] R. Sause, Corrugated Web Girder Fabrication, ATLSS Reports. ATLSS report number 03-19 2003.
[18] S.A. Ibrahim, W.W. El-Dakhakhni, Fatigue of corrugated web plate girders experimental study, J. Struct. Eng. 132 (9) (2006) 1371–1380.
[19] J.D. Harrison, Exploratory fatigue tests of two girders with corrugated webs, Br. Weld. J. 12 (3) (1965) 121–125.
[20] H.-t. Chen, X.-q. Chi, Y. Huang, Shear strength of I-shaped steel plate girder with sinusoidally corrugated webs, J. Highway Transp. Res. Dev. 30 (5) (2013) 38–46.
[21] R.G. Driver, H.H. Abbas, R. Sause, Shear behavior of corrugated web bridge girders, J. Struct. Eng. 132 (2) (2006) 195–203.
[22] Y. Guo, Q. Zhang, W. Xiaoan, A theoretical and experimental study of the shear strength of H-shaped members with sinusoidal corrugated webs, China Civil Eng. J. 43 (10) (2010) 45–52.
[23] S.-D. Shon, M.-N. Yoo, S.-J. Lee, J.-W. Kang, A comparative study on shear bucklng and interactive buckling characteristics of trapezoidal and sinusoidal corrugated steel plate, J. Architect. Inst. Korea Struct. Const. 31 (4) (2015) 39–46.
[24] G. Kiymaz, E. Coskun, C. Cosgun, E. Secklin, Transverse load capacity of sinusoidally corrugated steel web beams with web openings, Steel Compos. Struct. 10 (1) (2010) 69–85.
[25] H. Pasternak, P. Branka, Carrying capacity of girders with corrugated webs, Light-Weight Steel and Aluminum Structures: ICSAS '99, Cardiff, 1999.
[26] H. Pasternak, Girders with sinusoidally corrugated webs - Load carrying capacity and stability, Proceedings: 2004 Annual Stability Conference, March 24–27, 2004, Long Beach, California: reports on current research activities, Long Beach, 2004.
[27] Z. Zhang, S. Pei, B. Qu, Cantilever welded wide-flange beams with sinusoidal corrugations in webs: full-scale tests and design implications, Eng. Struct. 144 (2017) 163–173.
[28] H. Pasternak, J. Robra, V. Bachmann, Sinusoidal corrugated beams with increased web thickness - manufacturing technology and load carrying capacity, Bauingenieur 84 (2009) 415–419.
[29] W. Siokola, Corrugated web beam - production and application of girders with corrugated web, Der Stahlbau 66 (9) (1997) 595–605.
[30] American Association of State Highway and Transportation Officials, AASHTO LRFD Bridge Design Specifications, 8th edition AASHTO, 2017.
[31] E. Gerbo, A. Thrall, B. Smith, T. Zoli, Full-field measurement of residual strains in cold bent steel plates, J. Constr. Steel Res. 127 (2016) 187–203.
[32] Dassault Systemes, Abaqus 2017 Documentation, 2017 [Online]. [Accessed 2019].
[33] C. Yoo, S. Lee, Mechanics of web panel postbuckling behavior in shear, J. Struct. Eng. 132 (1) (2006) 1580–1589.
[34] Eurocode 3, Design of Steel Structures: Part 1.2 General Rules - Structural Fire Design, BSI, London, 2001.
[35] M.E.M. Garlock, S. Quiel, P. Wang, J. Alós-Moya, J. Glassman, Postbuckling mechanics of square slender steel plate in pure shear, Eng. J. 56 (1) (2019) 27–46.
[36] P. Wang, K. Augustyn, A. Gomez, S. Quiel, M. Garlock, Influence of boundary conditions on the shear post-buckling behavior of thin web plates, Conference Proceedings of the 2019 SSRC Annual Stability Conference, St. Louis, MO, 2019.
[37] J. Glassman, M.E.M. Garlock, E. Aziz, V.R. Kodur, Modeling parameters for predicting the postbuckling shear strength of steel plate girders, J. Constr. Steel Res. 121 (2016) 136–143.
[38] A. Gomez, Web Out-of-Straightness in Plate Girders: Methodology for Measurements and Effects on Shear Capacity, Princeton University, Princeton, 2020.
[39] AASHTO/AWS D1.5M/D1.5.2010, Bridge Welding Code, 6th edition AASHTO, 2010.
[40] J.D. Glassman, M.E.M. Garlock, A compression model for ultimate postbuckling shear strength, Thin-Walled Struct. 102 (2016) 258–272.
[41] FHWA, Standard plans for highway bridges, Struct. Steel Superstruct. 2 (1982).
[42] T. Höglund, Shear buckling resistance of steel and aluminum plate girders, Thin-Walled Struct. 29 (1) (1997) 13–30.
[43] A. Daley, D. Davis, D. White, Shear strength of unstiffened steel I-section members, J. Struct. Eng. 143 (3) (2017).
[44] AISC, Specification for Structural Steel Buildings, American Institute of Steel Construction, Chicago, 2016.
[45] D.W. White, M.G. Barker, Shear resistance of transversely stiffened steel I-girders, J. Struct. Eng. 134 (9) (2008) 1437–1449.
[46] CEN, Part 1–5: Plated structural elements, EN 1993–1–5 (2006) (English): Eurocode 3: Design of steel structures. , CEN, 2006.